Environmental Science Nano

Rapid Characterization of Arsenic Adsorption on Single Magnetite Nanoparticles by Collisions at Microelectrodes

Journal:	*Environmental Science: Nano*
Manuscript ID	EN-ART-03-2020-000336.R1
Article Type:	Paper

Environmental significance statement

Magnetite nanoparticles (NPs) are being studied as adsorbents for the removal of arsenic contaminants, but their adsorption properties can vary greatly depending on the size, surface coatings and presence of natural organic materials. This work describes a rapid and inexpensive approach to screen NPs for their ability to bind As^{3+} and predict the removal capacity of NP candidates before being implemented in environmental decontamination systems.

The method is based on the principle of the newly developed single particle collision electrochemistry that allows electrochemical measurements of redox processes at single NP surfaces. In this work, we demonstrate the ability of this method to probe electrochemical oxidation of the surface adsorbed As^{3+} on magnetite NPs as the particles collide with a gold microelectrode. Unlike spectroscopic approaches, single particle electrochemistry provides information on both the redox and surface sorption processes occurring at the contaminant/NP interface in aqueous solutions, without any treatment of the sample. The method can be used as a rapid measurement tool to evaluate heavy metal ion adsorption on nanomaterial sorbents for environmental monitoring and remediation applications.

Rapid Characterization of Arsenic Adsorption on Single Magnetite Nanoparticles by Collisions at Microelectrodes

Farideh Hosseini Nourei, Daniel Andreescu and Silvana Andreescu*

Department of Chemistry and Biomolecular Science, Clarkson University, Potsdam, NY, 13699-5810, USA.

E-mail: eandrees@clarkson.edu; Tel: +(315) 268 2394

ABSTRACT

We describe a rapid and sensitive electrochemical approach to evaluate the interaction of arsenite (As^{3+}) with magnetic Fe_3O_4 nanoparticles (MNPs) by single particle collision electrochemistry (SPCE). The method is based on direct measurements of the (As^{3+}) adsorbed on single MNPs, quantified via the oxidation of As^{3+} to As^{5+} at 0.4 V *vs.* Ag/AgCl, as the As-MNPs collide with a gold microelectrode (AuME). Measurement of the intensity of current spikes and the charge passed per impact spike provides a measure of As^{3+} content adsorbed per each MNP. The total calculated charge passed at AuME was monitored over 400 s collision time and the As^{3+} adsorption was quantified at different pH and environmental conditions. The charge increased significantly for MNPs exposed to a natural organic material, humic acid (HA), at concentrations of up to 5 ppm, and when the pH of the solution was between 6 and 8, indicating enhanced adsorption. The concentration of As^{3+} (0.013 - 0.036 fM As/MNP) was found to correlate well with the initial concentration of As^{3+} in solution (0.001 – 10 μM), suggesting that the method can also be used as an analytical tool to determine As contamination in environmental samples. The results were confirmed with spectroscopic techniques and demonstrate As^{3+} adsorption. Overall, this study demonstrates the capability of SPCE to fundamentally probe the surface properties of magnetite with high resolution and elemental specificity allowing a direct ultrasensitive assessment of the As^{3+} loading on individual MNPs. This approach could be used as a simple cost effective and fast screening tool to evaluate heavy metal ion adsorption on nanomaterial sorbents for environmental monitoring and remediation applications.

KEYWORDS: single nanoparticle collision electrochemistry (SPCE), environmental redox processes, arsenic – humic acid – magnetite interactions

Novelty of the work

A rapid and inexpensive method to analyze redox properties of magnetite nanoparticles and quantify arsenic adsorption by single particle collision electrochemistry.

Introduction

Arsenic (As) contamination in water and soil is a serious environmental problem worldwide. Main causes of As pollution are gold mining, non-ferrous smelting, industrial manufacturing, and the use of arsenical pesticides and herbicides. The most common As species are the inorganic arsenite (As^{3+}) and arsenate (As^{5+}), with As^{3+} having the highest toxicity. The World Health Organization (WHO) guideline value indicating the maximum limit of As contamination in drinking water is 10 μg/L or 10 ppb[1] but reaching the WHO limit is a challenge for many water treatment systems, especially small drinking water systems. Therefore, there is a need to develop more effective technologies to reduce the long term effects due to As exposure. Adsorption onto various types of sorbents including clays, resins, gels, biomass, carbons and oxides is one of the primary method to remove As.[2] More recently, nanomaterial sorbents which include different types of nanoparticles (NPs) and nanofibers (carbon nanotubes, Al_2O_3, TiO_2, CuO, ZnO, CeO_2, SiO_2, MnO_2, etc.) have attracted a great deal of attention due to their high adsorption capabilities for heavy metal removal.[3]

Among the different types of materials, the iron based materials[4] and their nanoscale counterparts such as magnetite Fe_3O_4 NPs (MNPs) produced as stable monodispersed colloids with tunable surface functionalities[5] are of particular interest due to the strong interaction between As and Fe, and the magnetic properties of MNPs. This high affinity was used to create adsorbents with high removal efficiency through their high specific surface area[6] and enable facile separation and analysis through their magnetic properties.[7] The mechanism of As adsorption on magnetite is thought to involve the oxidation of As^{3+} to As^{5+} at the NP surface by the dissolved oxygen in water[8], followed by its reduction back to As^{3+} through a reaction with Fe^{2+} or electrons.[9] Adsorption is significantly affected by the presence of natural organic material (NOM) that is

commonly present in natural water ecosystems, interfering or enhancing the adsorption process.[10, 11,12] The NOM concentration in surface water ranges from 0.1 to 20 ppm and its content is mainly represented by humic acid (HA) as major component.[13] Due to his polyfunctionality (carboxylic, phenolic, amino, carbonyl, hydroxyl groups), HA is an anionic polyelectrolyte at all pH values, which make HA a powerful natural chelating agent. HA has high affinity for Fe_3O_4 NPs, adsorbing to their surface through a ligand exchange mechanism between carboxyl (HA) and surface hydroxyl groups (MNPs).[14] Arsenic species can react with HA through the deprotonated functional groups within the HA and the process is dependent on pH and ionic strength.[15] In the presence of Fe, the dissolved NOM can bind a considerable amount of As^{3+} through As-Fe-NOM complexation,[16] and therefore HA can simultaneously form complexes with metal ions and coat the MNP surface. In general, HA-MNPs have higher adsorption capacity as compared with HA or iron oxides alone.[17, 18] HA coated MNPs have showed high removal efficiency for Hg, Pd, Cd and Cu ions from water (over 95%).[19] For Cr^{6+}, a simultaneous adsorption and reduction to Cr^{3+} on the surface of HA-Fe_3O_4 with no transformation of the magnetite core was reported.[20] Recently, it was found that when the HA concentration was higher than 3.5 mg/L, the Cr^{3+}-NOM-Fe can form colloids at anoxic-oxic interfaces, controlling the fate and transport of Cr.[21] The HA-MNPs was found to be an effective magnetic adsorbent for As^{3+} removal.[22] Using a binary graphene – magnetite nano-composite coated with HA, the As removal efficiency was two times higher at pH 7.[23]

Traditionally, MNPs characterization and their surface adsorption mechanism are studied by spectroscopic methods including UV, Raman,[22] FTIR,[24] X-ray photoelectron (XPS)[22, 25] and X-ray absorption (XAS) spectroscopy.[26, 27] These methods are time-consuming, require trained personnel and are not readily available. While As adsorption on MNPs has been studied previously using spectroscopic procedures, the dynamic nature of these processes, the speciation and the amount of As removed per individual particles have not been studied quantitatively. Herein, we propose the use of SPCE as a new method for the detection and characterization of heavy metals adsorption on MNPs. SPCE monitors redox processes involving single particles interacting with an ME. The collision current – time *(i-t)* responses are either 'staircase' or 'spike' shape signals and provide mechanistic and quantitative information regarding the surface properties, reactivity, size and coating of NPs.[28,29]

Using SPCE, we studied the As^{3+} uptake by magnetite NPs in the absence and presence of

HA. The analysis involves the quantification of the oxidation (As^{3+}/As^{5+}) currents (spikes number, intensity, charge) recorded during random collisions between MNPs exposed to As and a gold microelectrode (AuME). Calculating the average charge per impact or the total charge enabled direct assessment of As adsorption under varying pH, As and HA concentrations. Until now, monitoring As adsorption was performed mainly by spectroscopic techniques. The new method proposed here monitors As adsorption on the surface of individual MNP and provides a rapid screening test to assess the ability of these particles to bind and remove As. This approach can be applied to screen particles for their ability to bind As^{3+} and predict the removal capacity of NP candidates before being implemented in environmental remediation applications. Although a specific application for the study of As onto MNPs is presented here, the method could be extended broadly to study other heavy metals and nanomaterial sorbents.

Experimental Section

Reagents and materials. Sodium arsenite ($NaAsO_2$), humic acid, sodium chloride (NaCl), ferrocenemethanol 97% (FeMeOH), sodium sulfate (Na_2SO_4), ferrous and ferric chlorides ($FeCl_2$ $4H_2O$ and $FeCl_3$ $6H_2O$) were purchased from Sigma Aldrich. Ammonium hydroxide (NH_4OH – 30%) and nitric acid (HNO_3 – 60%) were obtained from Fisher Sci. Arsenic standard solution (1000 µg/ml) was purchased from Alfa Aesar. PFA-coated gold wire (AuME, ϕ = 76.2 µm) used for gold microelectrode fabrication was purchased from A-M Systems (cat # 751000). Phosphate buffer (PB) 0.1M with a pH of 7.5 was prepared using sodium phosphate (monobasic and dibasic) (Fisher Sci.). Gold disc electrodes (AuE, ϕ = 2 mm) and Ag/AgCl reference electrodes were purchased from CH Instruments. To manufacture the AuMEs, silver conductive epoxy (MG Chemicals) and non-conductive epoxy (Devcon) were used. All solution were prepared with deionized (DI) water (Millipore, Direct-Q System) with a resistivity of 18.2 Ω cm.

Magnetite NPs synthesis. Magnetite NPs used in collision experiments were prepared by hydrothermal (80 C) co-precipitation process of Fe^{2+} and Fe^{3+} ions (molar ratio 1:2) under alkaline conditions (pH 10) according to a previous procedure.[30] At the end, the MNPs were magnetically separated, washed a few times with DI water, filtered and dried under vacuum at 70 C for 24h. TEM images shown monodispersed NPs with an average size of ~10 nm (**Figure S1**). The crystalline structure of MNPs, was confirmed by the X-ray diffraction (XRD) analysis. The XRD

pattern (**Figure S2**), illustrates the Braggs reflections associated with the face centered cubic (*fcc*) structure of magnetite (JCPDS file 19-0629). The crystallite size of MNPs calculated with Debye-Scherrer equation from the XRD plot was 9.25 nm, comparable with the size obtained from the TEM image.

Instrumentation. Electrochemical experiments were performed using a CHI800 (CH Instruments Inc.) connected with a picoamp booster (CHI201). The particles size distribution and the zeta potential were measured with a Brookhaven ZetaPals analyzer. Atomic absorption spectroscopy (AAS) measurements were performed with AAnalyst 600 (Perkin Elmer) graphite furnace spectrometer. The XRD analysis was performed with X'Pert X-ray diffractometer (PANalytical) using Cu $K_{\alpha 1}$ radiation source. The XPS analysis was performed with a Kratos AXIS Ultra DLD system having a monochromatic Al K_{α} X-ray source operated at 15 keV and 150W and the pressure below $1x10^{-9}$ mbar. Photoelectrons were collected at a 45° emission angle with respect to the surface. A hemispherical analyzer determined the electron kinetic energy, using pass energy of 160 eV for wide/survey scans, and 40 eV for high-resolution core level scans. The XPS spectra analysis was performed with XPSPEAK 4.1 software.

Sample preparation. The arsenic adsorption experiments were performed in 25 mL flasks using Fe_3O_4 dispersion (1 mg/ml), containing As^{3+} (0.001 - 100 μM) and HA (1 – 50 ppm) prepared in DI and mixed 24 h on a rocking shaker BioRocker (labForce). The NPs were separated from the supernatant by centrifugation followed by washing with DI (twice). At the end, the particles were redispersed in 1 ml DI (stock solution). For collision experiments, 100 μL of MNPs stock solution (1 mg/ml) was added in 4 ml 0.1M PB (pH 7.5). The concentration of magnetite NPs in the electrochemical cell was 24.4 μg/ml (104 μM). A diagram illustrating the sample preparation steps is shown in Supporting Information (SI) section (**Scheme S1**).

Analytical measurements. For FTIR, XRD and XPS measurements the samples were in dry state. The arsenic content present in supernatants after adsorption experiments was measured by AAS. The standard calibration curve was carried out for As concentrations in the range of 0.1 to 10 μM with the solutions prepared in 0.5% HNO_3 (**Figure S3**). Zeta potential (ζ) of NPs (0.1 mg/ml) was measured in 1mM NaCl (**Figure S4**). The chosen pH of solution was adjusted with either NaOH or HCl. All electrochemical experiments were performed in a three electrodes electrochemical cell placed in a Faraday cage (CH Instruments) located on a vibration-proof platform (Vibraplane).

The cell is containing either an AuE or an AuME as working electrode, an Ag/AgCl as reference electrode and a platinum wire as counter electrode. All potentials were referred to the Ag/AgCl reference electrode. For all cyclic voltammetry (CV) experiments, the potential scan starts from -0.9 V with initial 10 min nitrogen purged in PB solution. For collisions measurements, prior each experiment, the electrochemical cell was soaked in aqua regia and thoroughly rinsed with DI.

The AuME used as working electrodes was fabricated by inserting the PFA-gold wire in a capillary glass tube (Corning). The end that is going in solution was sealed with nonconductive paste, leaving ~ 10 mm free extended wire. A detailed fabrication procedure of MEs is presented in our recent study.[31] Each experiment was carried out in triplicates with a fresh electrode surface by cutting the wire. The collision experiments were performed at +0.4V, for maximum 400s in 0.1 M PB (pH 7.4) as electrolyte. CV tests were completed with a AuE (ϕ = 2 mm). The AuEs were polished with alumina, sonicated, rinsed with DI water and dried. The As-MNPs modified AuEs were made by drop-casting of 10 μL As/MNPs dispersion onto electrode surface and dried in an oven at 80 °C for 10 minutes. The electrodes were allowed to cool at room temperature for 2 minutes before use.

Results and Discussion

In this study, we evaluate the ability of the SPCE method to determine the interaction of As^{3+} with MNPs and demonstrate the utility of this approach as a tool to rapidly screen sorbents for their arsenic removal capacity. SPCE signals of the MNPs with an AuME are used to monitor the As^{3+} content adsorbed on each NPs in the presence and absence of HA. It is known that lower size MNPs adsorb a higher amount of As than their microscale counterpart. For example, when using 1 mg/mL MNPs and 6.68 μM As, the removal efficiency was over 99% for 12 nm MNPs and 25% for 300 nm MNPs.[7, 32] Therefore, we used in this study MNPs with an average size of ~10 nm as seen in the TEM images (**Figure S1**). The removal efficiency for two As concentrations (1 and 10 μM) by MNPs (1 mg/ml) was initially evaluated by AAS using a calibration range of 1- 100 μM (**Figure S3**). For 1 μM As^{3+} solution and 24 h incubation with MNPs, there was no residual As content detected in the supernatant, indicating that the entire amount of As was adsorbed by the MNPs. When 10 μM As was tested, the As concentration in supernatant was 0.55 μM (**Table S1**),

representing 94.5% removal, in line with previous studies.[33] To evaluate possible As^{3+} desorption, the two washing solutions were analyzed by AAS and no As was found in any of the solutions.

To determine the optimal potential for the SPCE measurements, CVs were recorded in 0.1 M PB (pH 7.5) in the presence of As-MNPs, and As^{3+} solution (2 mM) as control, using a commercial AuE (ϕ = 2 mm) with the MNPs drop casted onto the surface (**Figure 1)**. The CV of bare AuE (**Figure 1 - black**) shows the specific current evolution profile of polycrystalline Au surface displaying AuO formation at 1.0 V followed by its reduction at +0.47 V. The preceding oxidative peak at +0.87 V corresponds to Au-OH oxidation formed as an intermediate during AuO formation.[34] When As^{3+} is present in solution, the CV shows three additional peaks at -0.49 V, -0.17 V and +0.48 V respectively (**Figure 1 - blue**). The peak at -0.17 V during the anodic scan corresponds to the oxidation of newly formed As^0 to As^{3+}, followed by its oxidation to As^{5+} at +0.48 V. The cathodic peak at -0.49 V in the reverse scan is associated to As^0 formation from the $As^{3+(5+)}$ reduction process.[35] The CV of the drop casted As-MNPs has a similar profile as the As solution, with an extra pair of peaks at + 0.017 V and -0.28V corresponding to the Fe^{2+}/Fe^{3+} oxidation-reduction process.[36] These findings prove the ability of the electrochemical measurements to evaluate the As content present onto the MNPs surface. Based on these measurements, a potential of +0.40 V that corresponds to the As^{3+}/As^{5+} oxidation process was selected for the collision experiments.

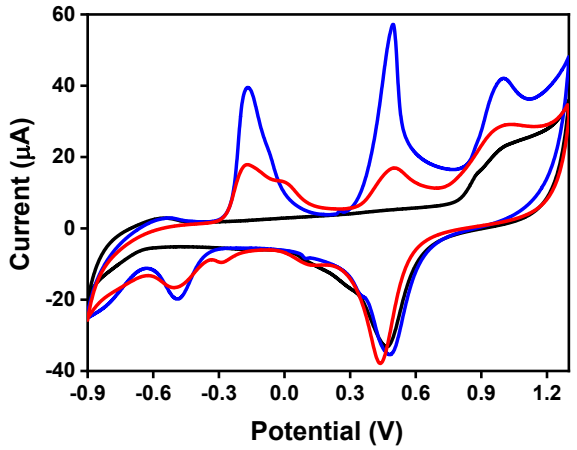

Figure 1. The cyclic voltammograms of AuE (black), As-MNPs modified AuE (red) and the AuE CV of 2 mM As^{3+} (blue) in 0.1M PB (pH 7.5) *vs*. Ag/AgCl as reference electrode. The scan rate was 50 mV/s.

SPCE measurements to monitor As adsorption.

In the first set of experiments, SPCE was used to determine the adsorption capacity (surface loading) of MNPs for As^{3+} under different pH conditions. **Figure 2** illustrates the SPCE chronoamperograms of F_3O_4 modified with As^{3+} at different pH values, monitored with the AuME at an applied potential of + 0.4 V. The MNPs (1 mg/ml) were exposed to As^{3+} solution (10 µM) and monitored after 24 hours incubation. After this time, the charge passed per impact spike remained constant. The chronoamperogram of unmodified MNPs did not show any oxidative currents; *e.g.* the current noise intensity level was ~1 pA (**Figure S5A**). Therefore, in this work, only peaks with current intensity values higher than 3 pA which represent more than three times the value of signal/noise (S/N) ratio were considered. Each SPCE experiment was conducted with a freshly renewed electrode.

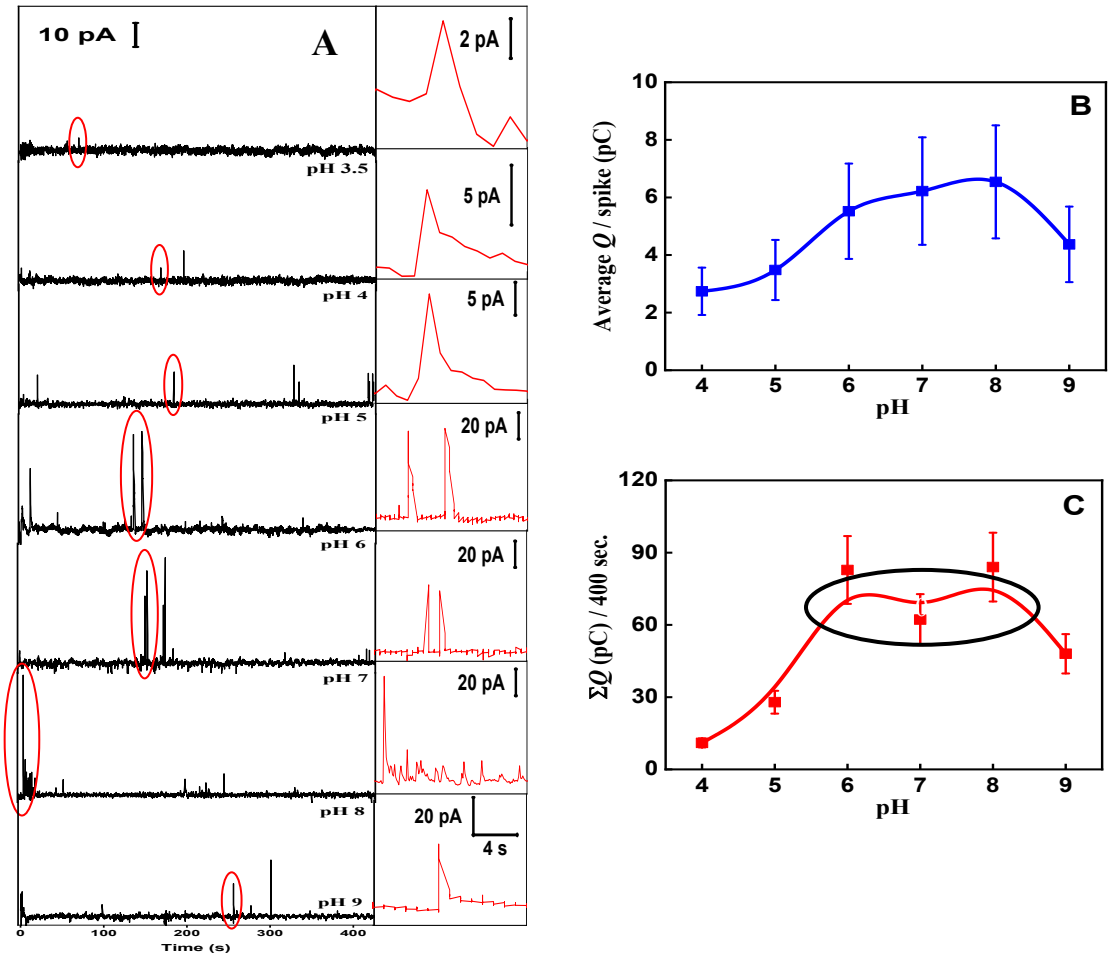

Figure 2. The chronoamperograms of As^{3+} oxidation process during nanoparticle collisions (A), the average charge per spike (B), the total charge of collisions (C) recorded for 400 s with As-MNPs prepared at different pH values.

To test if the surface of the renewed electrodes is reproducible, the experimental radius (r) of the Au planar electrode was calculated with *eq. 1*,[37] using the diffusion limited current *(i_{ss})*. The i_{ss} value was obtained from the electrode CV carried out in 2 mM FcMeOH with 0.1M Na_2SO_4 (**Figure S6**).

$$i_{ss} = 4\, n\, F\, D\, C\, r \qquad (1)$$

(*where*: n is the number of electrons transferred per redox molecule, F is Faraday constant, D is the diffusion coefficient of FcMeOH ($D = 6.7 \times 10^{-6}$ cm^2/s) and C is the FcMeOH concentration in solution)

The calculated electrode radius measured experimentally was 42.2 μm, close to the value provided by manufacturer (~ 39 μm), proving a reproducible electrode surface for every test. For each experimental condition, the collision tests were performed with at least three different electrodes.

SPCE measurements show a number of spikes-like signals, which are attributed to the oxidation of As^{3+} to As^{5+}, when the particles carrying the As^{3+} collide with the ME. According to the Pourbaix diagram, As^{3+} is present mainly as uncharged H_3AsO_3 when the pH is lower than 9 and $H_2AsO_3^-$ ($pK_a = 9.22$) when the pH is higher.[38] The zeta potential evolution of MNPs (0.1 mg/mL) as a function of pH is illustrated in **Figure S4**. The pH with point zero charge (pH_{pzc}) was 7.1. For As-MNPs prepared with 10 μM As, the ζ values were negative, when the pH is between 4 and 10. For As-MNPs prepared at pH lower than 5, the number of collisions recorded for 400 s was less than 8. The average oxidation current values was ~ 5 pA (**Figure 2A**) and the average charge integrated from each peak was ~ 3.5 pC (**Figure 2B**). For As-MNPs prepared at pH between 6 to 8, the average charge per impact is the highest (5.5 – 6.5 pC), as well as the oxidation current value (~ 20 pA). Since the distribution of average charge values is large, a more accurate evaluation can be made by considering the total collision charge recorded for the total 400 sec. As can be seen in **Figure 2C**, the total calculated charge passed at electrodes during 400 sec collision time is nearly identical (75 ± 9 pC) when the pH of the As solution was between 5.5 and 8.5 suggesting maximum As adsorption when the pH of solution is in this range. These results are in line with previous work stating a high affinity of As^{3+} for solids when the pH is over 6,[39] demonstrating the capability of SPCE to evaluate pH-dependent heavy metals adsorption.

Table S2 summarizes the electrochemical parameters extracted from the collision

measurements that allow us to calculate the amount of As^{3+} adsorbed onto each particle. Considering the charge resulted from the collision event and the number of electrons involved, the average number of As atoms present on single MNP can be calculated according with *eq*. 2.[40]

$$Q = n\ e\ N_{As} \qquad (2)$$

(*where*: n = 2, *e* = 1.6 x 10^{-19}C and N_{As} is the number of As atoms)

The As concentration found on the MNPs prepared at pH 7-8 was 0.032 fM, almost three times higher than the one prepared at pH 4 (0.014 fM) – **Table S2**. When the pH of the solution was 9, the As content on MNPs decreased by 30% (0.024 fM). As a result of these experiments, all future tests were carried out at pH 7.5, which is also representative for most aquatic environments. **Figure 3** illustrates the influence of the As-MNP concentration on the collision profile. As can be seen, the number of collisions increased with the As-MNPs concentration. The same trend was obtained considering the value of total charge passed at electrode for 300 s (**Figure 3C**).

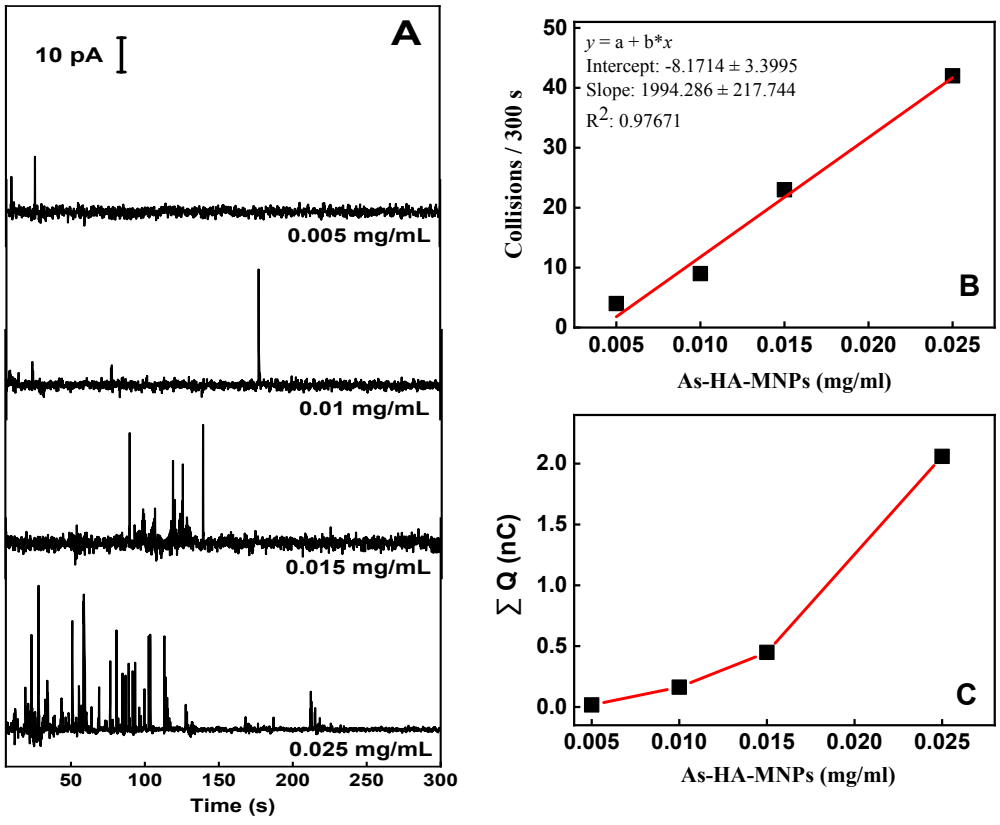

Figure 3. *I-t* profiles of arsenic oxidation with the concentration of As-MNPs varying between 0.005 and 0.025 mg/ml, recorded at +0.4 V (A) as well as the influence of their concentration in the number of collisions (B) or in the total charge recorded for 300 s (C).

However, for concentrations higher than 0.015 mg/ml, the recorded charge was higher but the As-MNPs start to agglomerate indicating a change in surface charge. The MNPs concentration used in further experiments to study the effect of HA and As^{3+} concentration was 0.015 mg/ml.

Effect of natural organic matter (NOM) on As adsorption on MNPs.

Further experiments were conducted to study the influence of NOM on As adsorption by MNPs. Humic substances such as fulvic acids (FAs), humic acids (HAs) and humin are commonly present in the environment and are known to adsorb to the surface of solid particles. Among NOM, HAs have a higher structural complexity that make them soluble at high pH and insoluble under acidic conditions (**Figure S7**). Adsorption of HA was found to increase the stability of MNPs dispersions in a wide range of pH and prevent aggregation induced by salts at neutral pH.[41, 42] However, when both As and NOM are present in solution, the competitive adsorption between HA and As is expected to lower the As^{3+} content adsorbed by MNPs.[43]

Before SPCE experiments, As adsorption to MNPs and HA-MNPs was studied by FTIR spectroscopy (**Figure S8)**. The IR spectra of all MNP samples show a splitted adsorption band in the region of 580 – 640 cm^{-1} associated to ν_1(Fe-O) vibration in tetrahedral and octahedral arrangements[44] and the presence of O-H stretching vibration at 3440 cm^{-1}. The IR spectrum of As-HA-MNPs shows the presence of the more specific bending vibrations of methyl and methylene groups at ~1380 cm^{-1} and the overlapping stretching vibration of the C-O from the different functional groups in HA ~ 1100 cm^{-1}. The plot is similar to the IR spectrum of bare HA proving a strong attachment between HA and MNPs. The IR spectrum of As-MNPs prepared in the absence of HA clearly illustrates a specific "splitted" band at ~ 825 cm^{-1} corresponding to As-O vibration. This splitting of ν(As-O) was associated with the presence of two types of As-O bonds: the first one at 820 cm^{-1} related with the surface complexed Fe-O-As and the second one at 841 cm^{-1} generated by the non-surface As-O bonds.[24] This bond is related to the As^{5+} sorption onto iron oxides, suggesting a possible chemical oxidation of As^{3+} to As^{5+} by the dissolved oxygen at neutral pH upon adsorption onto MNPs.[8] The spectrum of As-HA-MNPs has only one band for As-O vibration at a lower wavenumber value (811 cm^{-1}), that corresponds to As^{3+} sorption,[45] suggesting possible complexation of As^{3+} by HA without oxidation. These results indicate a competitive binding between HA and As, in which HA is initially adsorbed to the MNPs, after which the adsorbed HA layer binds As through its deprotonated carboxylic and phenolic –OH groups. The interaction involves a ligand exchange process through the phenolic groups and the formation of

a negatively charged adduct through the carboxylic groups.[11] The interaction of HA with both MNPs and arsenic affects the adsorption capacity of MNPs in presence of HA.[46]

We therefore used SPCE to study the influence of HA towards As adsorption at the single NP level. **Figure 4** shows the *I-t* profiles of the effect of different HA concentrations on the arsenic uptake by MNPs**.** For all experiments, the concentrations of As^{3+} (10 µM) and MNPs (1 mg/ml) were constant, and the HA concentration was varied from 1 to 50 ppm.

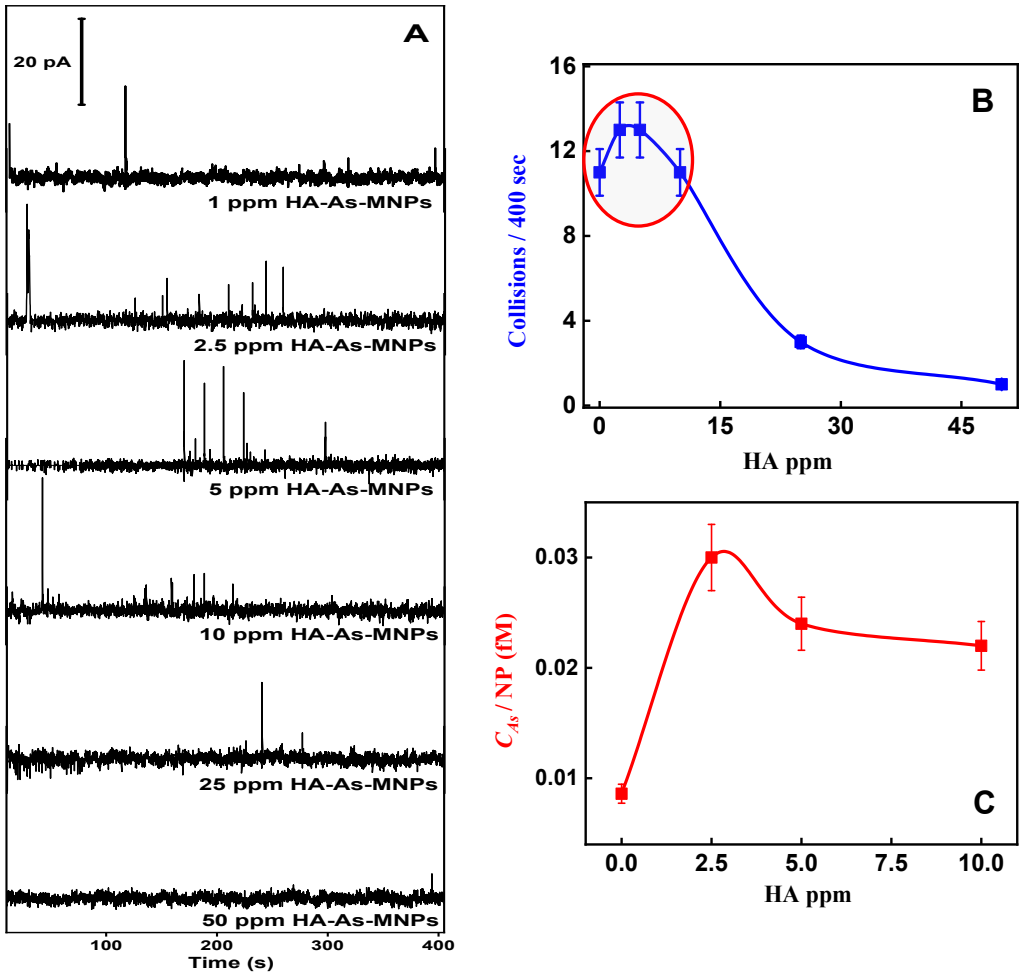

Figure 4. *I-t* graphs of As^{3+} oxidation involving As-MNPs and As-HA-MNPs (A), the average collisions number recorded for 400 sec (B) and the calculated As content per single NP (C) using different HA concentrations for NPs modification.

The chronoamperogram of HA-MNPs in absence of As^{3+} has no current spikes which is similar to the bare MNPs (**Figure S5B**) demonstrating the absence of any oxidation processes related to HA. For As-HA-MNPs samples prepared with HA in concentrations up to 10 ppm, the

number of collision events were nearly the same, 13 ± 4, regardless of the HA concentration. However, when the HA concentration was higher than 10 ppm, the number of collision decreased to ~ 3-4 for 25 ppm HA and almost ceased for 50 ppm (1-2) - **Figure 4B**. The average current intensity increased from ~ 8 pA in the case of As-MNPs with 1 ppm HA to ~ 19 pA for the NPs with 5 ppm HA. For HA concentration higher than 10 ppm, the current intensity decreased to ~ 12 pA (**Figure 4A**).

The HA concentration in the natural environment is below 10 ppm, for which the *I-t* measurements showed increased collision frequency, as the stability of the As-MNPs dispersion is preserved.[13] When the HA content is higher than 10 ppm, the collision frequency rapidly decreases. The decrease could originate from two causes: NPs agglomeration or the competitive adsorption between As and HA.[43] To assess a competitive adsorption mechanism, two As^{3+} concentrations (10 and 100 μM) were tested with either 5 or 50 ppm HA, and the residual As^{3+} amount was assessed by AAS. The HA-MNPs prepared with 5 ppm HA showed a removal efficiency of 97% from a solution of 10 μM As, slightly higher compared with the bare MNPs (94.5%) – **Table S1**. However, when the HA-MNPs were prepared with 50 ppm HA, the removal efficiency of 10 μM As^{3+} decreased to 90.1% suggesting a lower accessibility of As^{3+} ions to the MNPs surface. As expected, when the concentration of As is higher (100 μM), the removal efficiency decreased for both HA levels to 94.3% (5 ppm HA) and 89.3% (50 ppm) respectively. Interestingly, the removal efficiency (~94.3%) of 10 μM As^{3+} by bare MNPs was similar to that of 100 μM As^{3+} by HA-MNPs (5 ppm HA). This suggests a greater removal capacity of HA-MNPs as compared to the bare particles. High removal efficiencies by HA coated Fe_3O_4 NPs were also reported for Hg^{2+}, Pb^{2+}, Cd^{2+}, Cu^{2+}, Cr^{3+}.[19, 20] The particle size distribution (PSD) increased from 82 ± 13 nm (MNPs) to 188 ± 25 mm (As-MNPs), 121 ± 22 (HA-MNPs with 5 ppm HA) and 118 ± 18 nm (As-HA-MNPs with 5 ppm HA) respectively. These results indicate agglomeration of bare MNPs induced by As adsorption. When the MNPs are coated by HA, there is no increase in PSD, suggesting a stabilizing effect of HA.

Figures 4C shows the evolution of As content per particle (C_{As}/p) with respect to HA concentration, calculated using *eq*. 2, using the average transfer charge (Q). The corresponding electrochemical parameters are presented in **Table S3.** The average charge resulting from As exposed to HA-MNPs prepared in 1 ppm of HA was 1.66 pC, corresponding to 0.008 fM As content per each NP. For HA-MNPs with HA concentration up to 5 ppm, the charge increased to

5.72 pC (~ 0.03 fM As), followed by a slight decrease to 3.63 pC (0.024 fM As) when the MNPs were prepared with 10 ppm HA. These results correlate well with the AAS data and are consistent for HA concentrations below 10 ppm. The results also confirm binding of arsenite in the As^{3+} form to both HA[11] and iron oxides[24], with significantly higher efficiency to the HA-modified MNPs.

SPCE measurements were carried out at the potential corresponding to the oxidation of As^{3+} to As^{5+}. The As^{3+}/As^{5+} oxidation signals indicate that in these conditions (6-8 pH and 0-10 ppm HA) the As adsorbed on the MNPs is present predominantly as As^{3+} and that any possible chemical oxidation by the Fe_3O_4 would also involve reduction of the newly formed As^{5+} back to As^{3+}. Compared the two cases, the reduction of As^{5+} to As^{3+} or probably the limitation of initial As^{3+} oxidation, is more effective when the HA is present. However, in realistic environmental conditions with As concentrations less than 10 μM and a HA concentration below 10 ppm, the As^{3+} oxidation by Fe_3O_4 is drastically suppressed. To confirm the As^{3+} oxidation state onto MNPs and HA-MNPS, we used XPS to study As speciation and the redox processes involving As at the MNPs and HA-MNPs surface. Two different concentrations of As^{3+} (10 or 100 μM) and 5 ppm HA were used in these experiments. The high-resolution XPS spectra of Fe 2p, As 3d, C 1s, N 1s, O 1s are illustrated in **Figures S9-S11**, and the percentage of the elemental mass distribution is shown in **Table S4**. The changes in oxidation states of As and Fe were evaluated by deconvoluting the Fe 2p and As 3d peaks into their correspondent Fe^{3+}/Fe^{2+} and As^{3+}/As^{5+} component peaks and analyzing the area of each component. The percentages associated to the elemental mass content to each oxidation state of As and Fe are also shown in **Table S4**. The Fe 2p spectrum reveled the Fe $2p_{3/2}$ peaks at 710.5 eV (Fe^{2+}) and 712.7 eV (Fe^{3+}) and the Fe $2p_{1/2}$ at 724.2 eV (**Figure S9A**) and is similar for all MNPs tested.[22] While the C 1s spectrum can be deconvoluted in three distinct peaks: 284.7 eV (C-C), 286.1 eV (C-O), 288.3 eV (C=C) - **Figure S9B**, the O 1s spectrum has two components at 529.8 eV assigned to Fe-O (lattice oxygen in Fe_3O_4) and 531.4 eV associated with C-O bonds (**Figure S9C**). The initial iron content of unmodified MNPs was 68.6%. For modified NPs, the iron content progressively decreased to 63.7% as the concentration of As or As/HA increased, demonstrating their strong adsorption onto the MNPs surface. For As-MNPs, prepared in 10 μM As, the peak associated with As 3d at ~ 44eV, was not present. However, for MNPs exposed to the same As concentration in HA (5 ppm), the As 3d peak was present (**Figure S10A**) with an As content of 0.5% (wt). In addition, the presence of the N 1s peak at 400 eV associated to HA is an indication of simultaneous As and HA adsorption onto MNPs (**Figure S10B**). This

suggests an enhanced As adsorption when the HA is co-present. A similar trend was reported for Cd-HA-hematite, where the adsorption of Cd by hematite was increased by HA.[17] In order to obtain more information about As adsorption on the NP surface, the concentration of As was increased to 100 μM. In this case, the adsorbed As content increased from 0.5 to 3.7 (wt %). By deconvoluting the As 3d peak into As^{3+} – 44.1 eV and As^{5+} – 45.8 eV components, and calculating the peak area of each component, it was found that the sample contains 81% As^{3+} and 19% As^{5+} (**Figure S11A**). Concurrently, the Fe^{3+}/Fe^{2+} ratio slightly increased from 1.29 (As free MNPs) to 1.31 (**Table S4**). It is known that the direct oxido-reduction process between Fe (Fe_3O_4) and adsorbed As^{3+} is affected by oxygen.[9] The mechanism involves a simultaneous oxidation of As^{3+} and MNPs followed by reduction of the newly formed As^{5+} back to As^{3+} by the reactive oxygen species produced by Fe^{2+} oxidation. When HA (5 ppm) was used, the adsorbed As content increased from 3.7 to 4.8 (wt%). The As 3d peak (**Figure S11B)** featured the As^{3+} and As^{5+}. As compared with MNPs, the As^{5+} content in the HA-MNPs decreased from 19% to 15% and the Fe^{3+}/Fe^{2+} ratio decreased from 1.31 to 1.02, indicating a reduction of As^{5+} generated by the HA from the surface of HA-MNPs similar to that reported for the reduction of Cr^{6+} to Cr^{3+}.[20] Overall, the XPS results confirm the presence of a predominant As^{3+} oxidation state on the MNP surface, with higher As^{3+} content on the HA-MNPs, as measured by the electrochemical and SPCE data.

Quantitative aspects of SPCE: effect of arsenic concentrations.

Finally we evaluated the relationship between the As adsorbed onto the MNPs and the As in the initial solution and assessed the ability of the optimized SPCE method to provide a quantitative measure of the As content in solution. As concentrations ranging from 1 nM to 100 μM and 1 mg/ml MNPs at a pH of 7.5 were tested. **Figure 5** shows the *I/t* profile of collision frequency and the correlation between the current intensity and average charge per spike for varying As concentrations. A linear relationship was observed between the charge calculated from MNP collisions and the As concentration in the range 0.001 – 10 μM. For As concentrations higher than 10 μM, the dispersion loses stability and NP precipitate. The liner range covers representative levels of As in waters systems, including the EPA limit of 10 ppb (0.1338 μM). The current intensity increases from ~ 6 pA to ~ 30 pA with increasing the As concentration from 0.001 to 10 μM. In the same manner, the average charge per collision increased from 2.4 pC to 7.2 pC, and using the *eq*. 2, the As content per MNP was ranging from 0.013 to 0.036 fM (**Table S5**). The

error bars represent the number of three replicates The limit of detection (C_{LOD}) was calculated using the standard error of the regression ($3s_{y/x}$) and the slope (b) as followed $C_{LOD} = 3s_{y/x} \div b$. The C_{LOD} was 0.42 µM (31 ppb) using the current-based calibration curve and 0.48 µM (35 ppb) from the charge-based calibration curve.

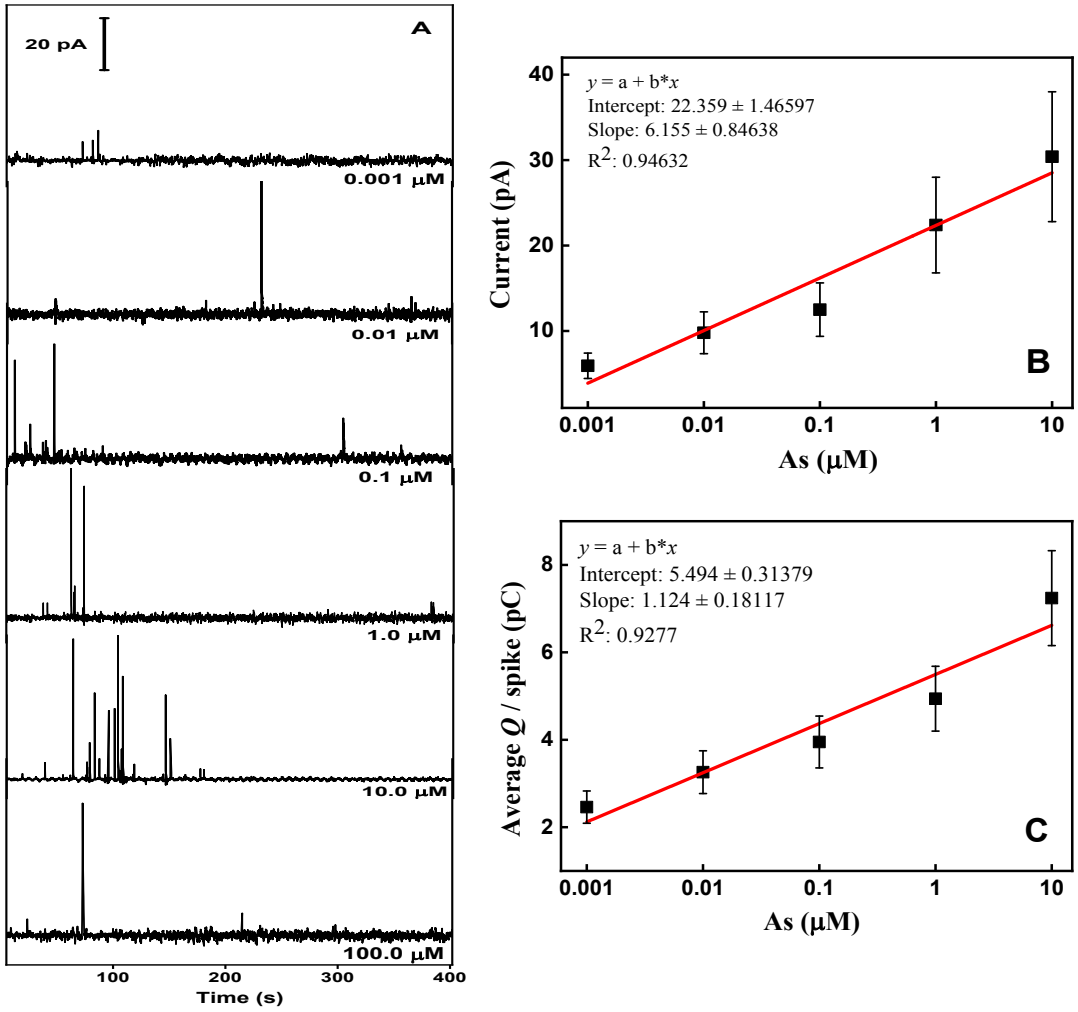

Figure 5. *I-t* profiles of collisions recorded at +0.45V using As-MNPs prepared with different As concentrations (A), and their correspondent linear range calibration curves associated with either current intensity (B) or total charge (C). The error bars represent the standard deviation from replicates.

These values cover the concentration range that is typically reported for As analysis using electrochemical sensors (0.008 – 200 ppb).[47] Although both methods are monitoring the oxidation of As^{3+} to As^{5+}, the electrochemical sensors quantify the As concentration in solution while the SPCE is measuring the As content adsorbed onto NP, which is useful for assessing the adsorption capacity of NP adsorbents and is important for environmental remediation applications. The

results demonstrate that it is possible to correlate the MNP average collision current or charge of the As adsorbed by the MNPs with the As concentration in solution. This dependency can be used to measure the As content in water systems and to evaluate the adsorption efficiency of MNPs sorbents.

Conclusion

In summary, we demonstrated the applicability of the SPCE technique to evaluate fundamental surface properties of Fe_3O_4 MNPs and their interaction with As^{3+}, by measuring the oxidation of As^{3+} to As^{5+} as the As-MNPs collide with an AuME. Using this approach, we designed a quantitative method that allows direct measurement of the As^{3+} adsorbed per each MNP particle by single particle collisions at AuMEs. Measurement of the intensity of current spikes and the charge passed per impact spike provided a measure of As^{3+} content adsorbed per each MNP. The method enabled a quantitative assessment of the effect of HA and pH on the adsorption process. A maximum adsorption (0.036 fM As/NP) was achieved at pH values between 5.5 and 8.5, three times higher than the one obtained at pH 4 (0.014 fM), as determined from the collision data. When HA is present, a higher amount of As was adsorbed on the MNPs surface, and the results were in line with conventional spectroscopic methods. Fast analysis of the adsorption capacity of these MNPs, and potentially of other NP systems can help in the identification and screening of sorbents considered as materials for membranes and filtration systems to remove As from contaminated waters. Overall, the work demonstrates the potential of SPCE as an analytical tool to determine the concentration of As in solution and adsorbed on MNPs. This approach could complement or bypass costly characterization methods and allow screening of NP sorbents for environmental remediation applications.

Author information

Corresponding Author *E-mail: eandrees@clarkson.edu

All authors have given approval to the final version of the manuscript.

Notes: the authors declare no competing financial interest.

Acknowledgements

This material is based upon work supported by the National Science Foundation (NSF) under Grant 1610281. Any opinions, findings, and conclusions or recommendations expressed in this material are those of the author(s) and do not necessarily reflect the views of the NSF.

References

1. A. H. Smith, P. A. Lopipero, M. N. Bates and C. M. Steinmaus, Arsenic Epidemiology and Drinking Water Standards, *Science*, 2002, **296**, 2145-2146.
2. D. Mohan and C. U. Pittman, Arsenic removal from water/wastewater using adsorbents—A critical review, *J. Hazard. Mater.*, 2007, **142**, 1-53.
3. I. Ali, New Generation Adsorbents for Water Treatment, *Chem. Rev.*, 2012, **112**, 5073-5091.
4. L. Hao, M. Liu, N. Wang and G. Li, A critical review on arsenic removal from water using iron-based adsorbents, *RSC Adv.*, 2018, **8**, 39545-39560.
5. W. Li, C. H. Hinton, S. S. Lee, J. Wu and J. D. Fortner, Surface engineering superparamagnetic nanoparticles for aqueous applications: design and characterization of tailored organic bilayers, *Environ. Sci. Nano*, 2016, **3**, 85-93.
6. S.-F. Lim, Y.-M. Zheng and J. P. Chen, Organic Arsenic Adsorption onto a Magnetic Sorbent, *Langmuir*, 2009, **25**, 4973-4978.
7. C. T. Yavuz, J. T. Mayo, W. W. Yu, A. Prakash, J. C. Falkner, S. Yean, L. Cong, H. J. Shipley, A. Kan, M. Tomson, D. Natelson and V. L. Colvin, Low-Field Magnetic Separation of Monodisperse Fe₃O₄ Nanocrystals, *Science*, 2006, **314**, 964-967.
8. G. Ona-Nguema, G. Morin, Y. Wang, A. L. Foster, F. Juillot, G. Calas and G. E. Brown Jr, XANES evidence for rapid arsenic (III) oxidation at magnetite and ferrihydrite surfaces by dissolved O2 via Fe2+-mediated reactions, *Environ. Sci. Technol.*, 2010, **44**, 5416-5422.
9. C.-H. Liu, Y.-H. Chuang, T.-Y. Chen, Y. Tian, H. Li, M.-K. Wang and W. Zhang, Mechanism of Arsenic Adsorption on Magnetite Nanoparticles from Water: Thermodynamic and Spectroscopic Studies, *Environ. Sci. Technol.*, 2015, **49**, 7726-7734.
10. W. Li, P. Liao, T. Oldham, Y. Jiang, C. Pan, S. Yuan and J. D. Fortner, Real-time evaluation of natural organic matter deposition processes onto model environmental surfaces, *Water Res.*, 2018, **129**, 231-239.
11. J. Buschmann, A. Kappeler, U. Lindauer, D. Kistler, M. Berg and L. Sigg, Arsenite and arsenate binding to dissolved humic acids: influence of pH, type of humic acid, and aluminum, *Environ. Sci. Technol.*, 2006, **40**, 6015-6020.
12. M. E. Peña-Méndez, J. Havel and J. Patočka, Humic substances - compounds of still unknown structure: applications in agriculture, industry, environment, and biomedicine, *J. Appl. Biomed.*, 2005, **3**, 13-24.
13. A. Rodrigues, A. Brito, P. Janknecht, M. F. Proença and R. Nogueira, Quantification of humic acids in surface water: effects of divalent cations, pH, and filtration, *J. Environ. Monit.*, 2009, **11**, 377-382.
14. B. Gu, J. Schmitt, Z. Chen, L. Liang and J. F. McCarthy, Adsorption and desorption of natural organic matter on iron oxide: mechanisms and models, *Environ. Sci. Technol.*, 1994, **28**, 38-46.
15. P. Warwick, E. Inam and N. Evans, Arsenics Interaction with Humic Acid, *Environ. Chem.*, 2005, **2**, 119-124.
16. G. Liu, A. Fernandez and Y. Cai, Complexation of Arsenite with Humic Acid in the Presence of Ferric Iron,

Environ. Sci. Technol., 2011, **45**, 3210-3216.
17. A. P. Davis and V. Bhatnagar, Adsorption of cadmium and humic acid onto hematite, *Chemosphere*, 1995, **30**, 243-256.
18. A. W. P. Vermeer, J. K. McCulloch, W. H. van Riemsdijk and L. K. Koopal, Metal Ion Adsorption to Complexes of Humic Acid and Metal Oxides: Deviations from the Additivity Rule, *Environ. Sci. Technol.*, 1999, **33**, 3892-3897.
19. J.-f. Liu, Z.-s. Zhao and G.-b. Jiang, Coating Fe3O4 Magnetic Nanoparticles with Humic Acid for High Efficient Removal of Heavy Metals in Water, *Environ. Sci. Technol.*, 2008, **42**, 6949-6954.
20. W. Jiang, Q. Cai, W. Xu, M. Yang, Y. Cai, D. D. Dionysiou and K. E. O'Shea, Cr(VI) Adsorption and Reduction by Humic Acid Coated on Magnetite, *Environ. Sci. Technol.*, 2014, **48**, 8078-8085.
21. P. Liao, C. Pan, W. Ding, W. Li, S. Yuan, J. D. Fortner and D. E. Giammar, Formation and Transport of Cr (III)-NOM-Fe Colloids upon Reaction of Cr (VI) with NOM-Fe (II) Colloids at Anoxic–Oxic Interfaces, *Environ. Sci. Technol.*, 2020, **54**, 4256-4266.
22. M. Rashid, G. E. Sterbinsky, M. Á. G. Pinilla, Y. Cai and K. E. O'Shea, Kinetic and Mechanistic Evaluation of Inorganic Arsenic Species Adsorption onto Humic Acid Grafted Magnetite Nanoparticles, *J. Phys. Chem. C*, 2018, **122**, 13540-13547.
23. B. Paul, V. Parashar and A. Mishra, Graphene in the Fe3O4 nano-composite switching the negative influence of humic acid coating into an enhancing effect in the removal of arsenic from water, *Environ. Sci. Water Res. Technol.*, 2015, **1**, 77-83.
24. S. Goldberg and C. T. Johnston, Mechanisms of Arsenic Adsorption on Amorphous Oxides Evaluated Using Macroscopic Measurements, Vibrational Spectroscopy, and Surface Complexation Modeling, *J. Colloid Interface Sci.*, 2001, **234**, 204-216.
25. R. M. Couture, J. Rose, N. Kumar, K. Mitchell, D. Wallschläger and P. Van Cappellen, Sorption of Arsenite, Arsenate, and Thioarsenates to Iron Oxides and Iron Sulfides: A Kinetic and Spectroscopic Investigation, *Environ. Sci. Technol.*, 2013, **47**, 5652-5659.
26. C. C. Fuller, J. A. Davis and G. A. Waychunas, Surface chemistry of ferrihydrite: Part 2. Kinetics of arsenate adsorption and coprecipitation, *Geochim. Cosmochim. Acta*, 1993, **57**, 2271-2282.
27. M. L. Farquhar, J. M. Charnock, F. R. Livens and D. J. Vaughan, Mechanisms of Arsenic Uptake from Aqueous Solution by Interaction with Goethite, Lepidocrocite, Mackinawite, and Pyrite: An X-ray Absorption Spectroscopy Study, *Environ. Sci. Technol.*, 2002, **36**, 1757-1762.
28. X. Xiao and A. J. Bard, Observing Single Nanoparticle Collisions at an Ultramicroelectrode by Electrocatalytic Amplification, *J. Am. Chem. Soc.*, 2007, **129**, 9610-9612.
29. D. Andreescu, K. A. Kirk, F. H. Narouei and S. Andreescu, Electroanalytic Aspects of Single-Entity Collision Methods for Bioanalytical and Environmental Applications, *ChemElectroChem*, 2018, **5**, 2920-2936.
30. S. H. Huang, M. H. Liao and D. H. Chen, Direct binding and characterization of lipase onto magnetic nanoparticles, *Biotechnol. Prog.*, 2003, **19**, 1095-1100.
31. K. A. Kirk, T. Luitel, F. H. Narouei and S. Andreescu, in *Nanoparticles in Biology and Medicine: Methods and Protocols*, eds. E. Ferrari and M. Soloviev, Springer US, New York, NY, 2020, DOI: 10.1007/978-1-0716-0319-2_24, pp. 327-342.
32. J. Mayo, C. Yavuz, S. Yean, L. Cong, H. Shipley, W. Yu, J. Falkner, A. Kan, M. Tomson and V. Colvin, The effect of nanocrystalline magnetite size on arsenic removal, *Sci. Technol. Adv. Mater.*, 2007, **8**, 71.
33. B. E. Monárrez-Cordero, P. Amézaga-Madrid, C. C. Leyva-Porras, P. Pizá-Ruiz and M. Miki-Yoshida, Study of the Adsorption of Arsenic (III and V) by Magnetite Nanoparticles Synthetized via AACVD, *Mater. Res.*, 2016, **19**, 103-112.
34. E. Rouya, S. Cattarin, M. L. Reed, R. G. Kelly and G. Zangari, Electrochemical Characterization of the Surface Area of Nanoporous Gold Films, *J. Electrochem. Soc.*, 2012, **159**, K97-K102.
35. T. D. Cabelka, D. S. Austin and D. C. Johnson, Electrocatalytic Oxidation of As (III) I. Voltammetric Studies at Pt Electrodes in, *J. Electrochem. Soc.*, 1984, **131**, 1595-1602.
36. R. Rawal, S. Chawla and C. S. Pundir, An electrochemical sulfite biosensor based on gold coated magnetic nanoparticles modified gold electrode, *Biosens. Bioelectron.*, 2012, **31**, 144-150.
37. A. J. Bard and L. R. Faulkner, Fundamentals and applications, *Electrochemical Methods*, 2001, **2**, 482.
38. N. Takeno, Atlas of Eh-pH diagrams, *Geological survey of Japan open file report*, 2005, **419**, 102.
39. S. Dixit and J. G. Hering, Comparison of Arsenic(V) and Arsenic(III) Sorption onto Iron Oxide Minerals: Implications for Arsenic Mobility, *Environ. Sci. Technol.*, 2003, **37**, 4182-4189.
40. Y.-G. Zhou, N. V. Rees and R. G. Compton, The electrochemical detection of tagged nanoparticlesvia particle-electrode collisions: nanoelectroanalysis beyond immobilisation, *Chem. Commun.*, 2012, **48**, 2510-

2512.
41. E. Illés and E. Tombácz, The effect of humic acid adsorption on pH-dependent surface charging and aggregation of magnetite nanoparticles, *J. Colloid Interface Sci.*, 2006, **295**, 115-123.
42. E. Tombácz, I. Y. Tóth, D. Nesztor, E. Illés, A. Hajdú, M. Szekeres and L.Vékás, Adsorption of organic acids on magnetite nanoparticles, pH-dependent colloidal stability and salt tolerance, *Colloids Surf. A Physicochem. Eng. Asp.*, 2013, **435**, 91-96.
43. S. Yean, L. Cong, C. T. Yavuz, J. T. Mayo, W. W. Yu, A. T. Kan, V. L. Colvin and M. B. Tomson, Effect of magnetite particle size on adsorption and desorption of arsenite and arsenate, *J. Mater. Res.*, 2005, **20**, 3255-3264.
44. S. J. Iyengar, M. Joy, C. K. Ghosh, S. Dey, R. K. Kotnala and S. Ghosh, Magnetic, X-ray and Mössbauer studies on magnetite/maghemite core–shell nanostructures fabricated through an aqueous route, *RSC Adv.*, 2014, **4**, 64919-64929.
45. D. L. Suarez, S. Goldberg and C. Su, in *Mineral-Water Interfacial Reactions*, American Chemical Society, 1999, vol. 715, ch. 8, pp. 136-178.
46. A. B. Giasuddin, S. R. Kanel and H. Choi, Adsorption of humic acid onto nanoscale zerovalent iron and its effect on arsenic removal, *Environ. Sci. Technol.*, 2007, **41**, 2022-2027.
47. S. Kempahanumakkagari, A. Deep, K.-H. Kim, S. Kumar Kailasa and H.-O. Yoon, Nanomaterial-based electrochemical sensors for arsenic - A review, *Biosens. Bioelectron.*, 2017, **95**, 106-116.